Interplay of magnetocrystalline and magnetoelastic anisotropy in epitaxial Co(10$\bar{1}$0) films

Gauravkumar Patel [1,2] Fabian Ganss [1] Lorenzo Fallarino [3] Gabriel Sellge [4] Mikel Quintana [5] René Hübner [1] Dirk Sander,[6] Olav Hellwig [1,4] Kilian Lenz [1] and Jürgen Lindner [1]

[1] *Helmholtz-Zentrum Dresden-Rossendorf, Institute of Ion Beam Physics and Materials Research, Bautzner Landstraße 400, 01328 Dresden, Germany*

[2] *Faculty of Physics, Dresden University of Technology, 01062 Dresden, Germany*

[3] *CIC energiGUNE, Parque Tecnológico de Álava, Albert Einstein 48, 01510 Vitoria-Gasteiz, Spain*

[4] *Institute of Physics, Chemnitz University of Technology, 09107 Chemnitz, Germany*

[5] *CIC nanoGUNE BRTA, E-20018 Donostia–San Sebastián, Spain*

[6] *Max Planck Institute of Microstructure Physics, 06120 Halle, Germany*

(Received 8 November 2024; accepted 10 February 2025; published 21 February 2025)

With the goal of creating an in-plane (IP) uniaxial anisotropy system, we deposited a thickness series of epitaxial Co(10$\bar{1}$0) films grown on Si(110) substrates with Ag(110) and Cr(211) buffer layers by magnetron sputtering. However, quantifying the IP magnetic anisotropy using ferromagnetic resonance measurements revealed a much more complex behavior than expected for a simple uniaxial system like hexagonally close-packed (hcp) Co. To understand the experimental results, an in-depth x-ray diffraction analysis of the film structure was performed. Even at a thickness of 100 nm, it revealed an anisotropic strain in the Co films, mainly within the Co basal plane, while the *c* axis remained mostly unaffected. Calculations show that such unrelaxed strain induces a significant magnetoelastic anisotropy, which counteracts the magnetocrystalline one and, as a result, reduces the overall effective anisotropy. A detailed analysis revealed that mainly the compressive strain along the Co[10$\bar{1}$0] out-of-plane direction is responsible for the observed magnetoelastic anisotropy, while the tensile strain along the Co[$\bar{1}$2$\bar{1}$0] IP direction only plays a minor role.

DOI: 10.1103/PhysRevB.111.054431

I. INTRODUCTION

The large uniaxial magnetic anisotropy [1] and large saturation magnetization [2] of Co make it a very important element for spintronic research and applications. Since the discovery of the giant magnetoresistance (GMR) effect [3], Co-based thin films have enabled GMR-based hard disk drive (HDD) sensors to read back data from the HDD media at an ever increasing storage density. Nowadays, Co-based thin films are proposed to improve spintronic devices such as magnetic random access memory (MRAM). The ultimate goal is to create a non-volatile memory that is fast enough to enable in-memory processing [4]. The most promising technology for this purpose is spin-orbit-torque (SOT) MRAM, which is supposed to achieve a shorter write time than the currently applied spin-transfer-torque (STT) MRAM [4,5].

However, there are still a few challenges with SOT-MRAM: If the magnetization of the storage layer is aligned perpendicular to the film plane, an additional small in-plane magnetic bias field is needed to break the reversal symmetry and achieve a deterministic switching process [6]. Aligning the magnetization in the film plane would solve this issue but requires a specific material design with an easy axis of magnetization within this plane. An elliptical footprint of the MRAM cell could provide this easy axis by its shape anisotropy but limits the scalability of the design and thus the achievable storage density [5,7,8]. This challenge could be addressed using hexagonal close packed (hcp) Co films with their *c* axis aligned in the film plane instead of perpendicular to it, providing the easy axis by magnetocrystalline anisotropy without any geometrical restriction [9,10].

Yang [11] developed an epitaxy process to grow Co films with the *c* axis in the film plane on Si(110) substrates using Ag(110) and Cr(211) as buffer layers. Instead of Cr(211), later NiAl(211) was also used as an underlayer, but it reduces the magnetic anisotropy [12]. Single-crystalline MgO(110) is an alternative substrate, but Si(110) wafers are readily available and inexpensive [13]. The epitaxial growth of in-plane (IP) oriented Co films comes with a small lattice mismatch with the seed layers [11,12,14,15], and the resulting strain gives rise to magnetoelastic anisotropy. A decrease in magnetic anisotropy from bulk values was observed in IP-oriented hcp Co films and assigned to the presence of stacking faults without analyzing the influence of magnetoelastic anisotropy [11,12,14,15]. This article discusses the contribution of magnetoelastic anisotropy caused by strain to the magnetic anisotropy of the IP Co films.

First, the theoretical formalism of the magnetoelastic anisotropy in (10$\bar{1}$0)-orientated Co is developed in Sec. II. Then, in Sec. III, the sample growth mechanism and an

in-depth structural characterization, including the strain determination along three important crystallographic directions by x-ray diffraction (XRD) is discussed. Section IV focuses on the ferromagnetic resonance (FMR) measurements of the Co films and improvements of the theoretical formalism in order to advance the understanding of the experimental FMR data.

II. MAGNETOELASTIC ANISOTROPY

To first-order, the magnetocrystalline anisotropy energy density (F_K) resulting from spin-orbit coupling in the hexagonal crystal structure of Co is given by [11]

$$F_K = -K_2 \cos^2\varphi, \tag{1}$$

where K_2 is the first order magnetocrystalline anisotropy constant. For $K_2 > 0$, the direction parallel to the crystallographic c axis would be an easy axis, and a hard axis results if $K_2 < 0$. The angle φ represents the IP azimuthal angle of the magnetization, with the magnetization being parallel to [0001] at $\varphi = 0$. In a strained system, the underlying hexagonal crystal structure is distorted and a strain-dependent correction to the magnetocrystalline anisotropy energy can be considered by expanding it into a Taylor series with respect to the strain tensor elements $_{ij}$ [16], as follows:

$$F = (F_K)_0 + \sum_{i\ j} \left(\frac{\partial F_K}{\partial\ _{ij}}\right)_0\ _{ij} + \cdots \tag{2}$$

Here, is the strain tensor, $_{ij}$ being its components. The first term $(F_K)_0$ is nothing but the magnetocrystalline anisotropy energy of the unstrained hexagonal structure as given by Eq. (1). The first-order strain correction to F_K is commonly known as magnetoelastic anisotropy energy density (F_{me}). The higher-order strain corrections in Eq. (2) are neglected, since the $_{ij}$'s are typically small, of the order of less than a few percent. The calculation of F_{me} for the hexagonal Co system was performed by Bruno [17] for the (0001) orientation by considering the first-order term in F_K. In our case, the hexagonal Co system was grown in a way that the c axis lies within the film plane, making the Co(10$\bar{1}$0) lattice plane the surface plane. Hence, a coordinate transformation is necessary to derive an expression for the F_{me} of (10$\bar{1}$0)-oriented Co. After simplification, it can be written for the azimuthal plane as follows (see the Appendix for the detailed calculation):

$$F_{\text{me}}^{(10\bar{1}0)} = \tfrac{1}{8}(8B_2\ _{xx} + B_1(11\ _{yy} - 3\ _{zz}) + 8B_3(\ _{yy} +\ _{zz}))\sin^2\varphi. \tag{3}$$

Here, $_{xx}$, $_{yy}$, and $_{zz}$ are the diagonal components of the strain tensor and represent the strain in x, y, and z directions of the film, respectively, as depicted in Fig. 1(b). B_i's are the magnetoelastic coupling coefficients. It is clearly observed that the first-order F_K term and the F_{me} term have the same symmetry. Similar results were already published by Kittel [16], where it were shown in detail that in the magnetoelastic equilibrium configuration, the strain depends on the crystallographic direction in such a way that the F_{me} term can be expressed in the same symmetry as F_K. Hence, one can write Eq. (2) as follows:

$$F = -(K_2 + K_{2\text{me}})\cos^2\varphi. \tag{4}$$

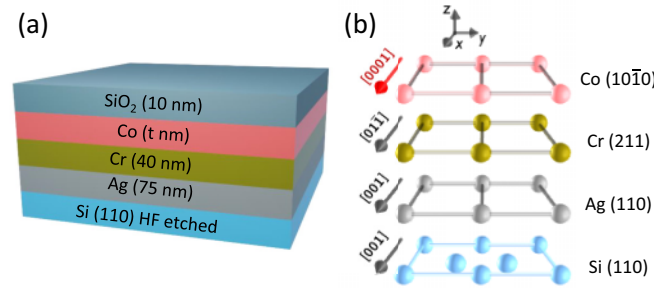

FIG. 1. (a) Sketch of the sample stack and (b) lattice plane relations for the epitaxial growth of Co(10$\bar{1}$0). The Co thickness t ranges from 5 to 100 nm. The directions in the Co films are defined as $X \parallel [0001]$, $Y \parallel [\bar{1}2\bar{1}0]$, $Z \parallel [10\bar{1}0]$.

From Eq. (3), it is clear that the prefactors depend on the B_i's, whose values are known [18,19] and listed in Table I in the Appendix for bulk hcp Co, as well as the strain components, which are measured, resulting in a constant prefactor for a given strain. Hence, they are simply denoted as $K_{2\text{me}}$, representing the first-order magnetoelastic anisotropy constant in Eq. (4).

III. FILM GROWTH AND STRUCTURAL CHARACTERIZATION

To achieve an epitaxial growth of hcp Co with the c axis oriented in the film plane by magnetron sputter deposition, we followed a procedure described in the literature [11,20]. The growth sequence and surface plane orientation of the different materials are shown in Fig. 1. A single-crystal Si wafer with (110) orientation is used as substrate. The native oxide on the wafer surface was removed by hydrofluoric acid etching right before inserting it into the ultrahigh vacuum (UHV) sputter chamber with a base pressure better than 10^{-8} mbar. Subsequently, 75 nm of Ag and 40 nm of Cr were deposited on the Si substrate. The dimensions of a 3×3 supercell of the Si interface match those of a 2×4 supercell of Ag almost perfectly. At the interface between Ag(110) and Cr(211), on the other hand, there is an almost perfect match in the [01$\bar{1}$] direction of Cr but a mismatch of -13.5% in the direction perpendicular to it. Regardless of this lattice mismatch, the Cr layer develops an epitaxial relation to the Ag layer [11,13,20] and provides an excellent seed layer for hexagonal Co with (10$\bar{1}$0) surface orientation. This orientation makes the crystallographic c axis, and hence the magnetic easy axis, lie within the film plane. For this study, different samples with varying Co thickness between 5 and 100 nm were grown using the same process. Further, all Co layers were capped with 10 nm SiO_2 to prevent oxidization after removal from the UHV chamber.

For structural characterization of the Co films, XRD measurements were performed in standard θ–2θ geometry ($\vec{Q} \parallel [10\bar{1}0]$, where $\vec{Q}$ is the x-ray scattering vector). Figure 2(b) shows the result of these XRD measurements for all Co thicknesses reported in this article. The observed Bragg peaks of Si(220), Ag(220), Cr(211), Co(10$\bar{1}$0), and Co(20$\bar{2}$0) indicate epitaxial growth throughout the layer stack, regardless of the anisotropic lattice mismatch at the Ag-Cr interface. The

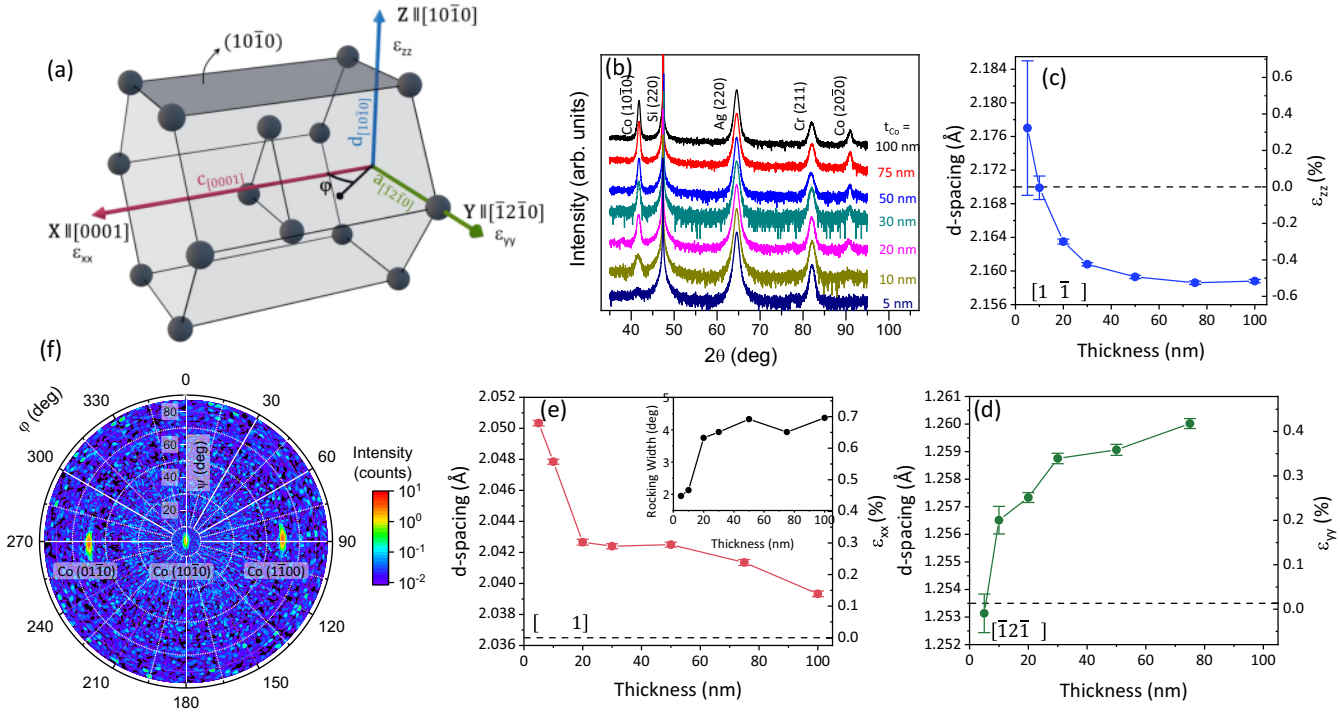

FIG. 2. (a) (10$\bar{1}$0) orientation of Co, with relevant directions and lattice planes highlighted. (b) XRD scans for the complete Co thickness series. (c)–(e) show the calculated d-spacing (left y axis) and strain (right y axis) in the directions [10$\bar{1}$0], [$\bar{1}$2$\bar{1}$0], and [0001], respectively. The strain in (c) and (d) changes its sign as the d-spacing crosses the reference value in both. The inset of (e) shows the width of the rocking curve measured within the film plane. (f) shows a pole figure for the 75-nm-thick Co film. The radial axis represents the tilt angle ψ from the surface normal, and the angular axis represents the azimuth rotation φ around the surface normal.

capping layer of SiO_2 grows amorphously, hence, it does not show any Bragg peak.

As the thickness of the Co layer increases, its Bragg peaks shifts slightly to higher angles. This shift is shown in Fig. 2(c) as a decreasing d-spacing, which represents the distance between parallel (10$\bar{1}$0) lattice planes, on the left y axis. The right y axis shows the corresponding strain as compared to the reference value, which is indicated as horizontal dashed line. The strain is calculated as $_{zz} = (d - d_0)/d_0$, where d is the measured and d_0 is the strain-free d-spacing. Thicker films deviate more from the latter and the strain $_{zz}$ reaches -0.5%. Unlike bulk materials, thin films are bonded to the underlayers. As a result of the lattice parameter mismatch, strain develops [21]. The strain usually relaxes as the film thickness increases. Nevertheless, the Co films reported here are still strained, even at 100 nm thickness. This unusual compressive strain for thicker films is most likely a result of the tensile strain that develops in the plane, as a result of the Poisson effect [22], which motivated us to investigate the development of the lateral strain in the Co films. The following investigation relies on in-plane XRD measurements, where instead of the lattice planes parallel to the surface, lattice planes perpendicular to the surface are investigated in the Bragg diffraction geometry. This is achieved by scanning the horizontal detector axis and the φ axis of a five-circle Rigaku SmartLab diffractometer in a 2:1 ratio [23]. Two lateral directions are individually probed this way: one being parallel to the c axis ($\vec{Q} \parallel [0001]$) and the other perpendicular to it ($\vec{Q} \parallel [\bar{1}2\bar{1}0]$). The profiles are shown in the Supplemental Material in Fig. S1 [24]. Figures 2(d) and 2(e) show the resulting d-spacing (left y axis) and strain (right y axis) for the Co ($\bar{1}2\bar{1}0$) and Co(0001) planes, respectively. The d-spacing of Co(0001) approaches the reference value at increasing thickness, but the d-spacing of Co ($\bar{1}2\bar{1}0$) deviates strongly from its reference value. It is evident that the surface plane of Co is anisotropically strained with $_{xx} \neq _{yy}$ at any given thickness up to at least 100 nm.

To further check the degree of preferred orientation of the Co(0001) planes, a rocking curve measurement in the IP geometry was performed as a φ scan, resulting in a Gaussian-like intensity profile. The full width at half maximum (FWHM) of this profile serves as a measure of twisting of crystallites [23]. The inset plot in Fig. 2(e) shows the measured FWHM, which is about 4° even for higher thickness. This means that the c axis is distributed mostly within $\pm 2°$ around its mean orientation, indicating a good alignment. Moreover, this is also confirmed by performing fast Fourier transform analysis of cross-sectional high-resolution transmission electron microscopy (TEM) images. It shows that the different Co grains are twisted slightly; see Fig. S2 in the Supplemental Material [24]. To investigate the presence of other possible orientations of Co, a pole figure (PF) was created exemplarily for the 75 nm Co film and is shown as Fig. 2(f). The central red region represents intensity reflected by the Co(10$\bar{1}$0) planes, which is the same reflection as observed in Fig. 2(b). The PF shows two more reflections, Co(01$\bar{1}$0) and Co(1$\bar{1}$00), which are located at $\psi = 60°$ at opposite φ angles. The lack of further intensity peaks or circles at this or other ψ angles confirms the presence of only one orientation of Co.

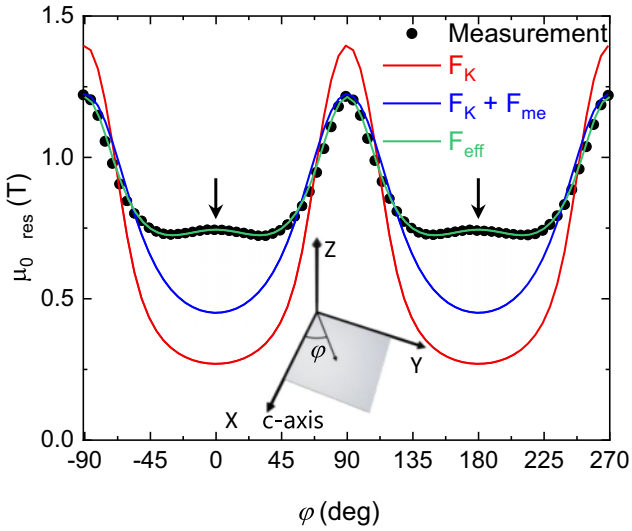

FIG. 3. FMR azimuthal scan of the 75-nm-thick Co film shown as dots. Red, blue, and green curves are the fitting model, considering the bulk magnetocrystalline anisotropy energy density (F_K), the sum of F_K and magnetoelastic anisotropy energy density (F_{me}), and the effective anisotropy considering first- and second-order anisotropy terms of F_K and F_{me}, respectively. It has to be kept in mind that the models are described as free energy density, but solved for the resonance field using Baselgia's equation [25] by considering all the energies within the magnetic system. The inset illustrates the respective coordinate system.

IV. FERROMAGNETIC RESONANCE MEASUREMENTS AND DISCUSSION

To characterize the strain-induced changes in magnetic anisotropy, FMR is used. The FMR measurement is performed using a vector network analyzer (VNA), which launches a microwave into a coplanar waveguide. The sample is placed flip-chip onto the waveguide and an external magnetic field within the sample plane is swept using an electromagnet. At resonance, the sample absorbs microwave power, which the VNA detects by means of the transmitted scattering parameter (S_{21}), which can be fitted using a complex Lorentzian line to determine the resonance field ($\mu_0 H_{res}$). Similar measurements were recorded for various IP angles (φ) at 45 GHz excitation frequency, and the resulting resonance fields are fitted and plotted in Fig. 3 for the 75-nm-thick Co film. At $\varphi = -90^\circ$ and for multiples thereof, where the external magnetic field is perpendicular to the c axis, $\mu_0 H_{res}$ shows maximum values indicating a magnetic hard-axis behavior. Uniaxial systems like Co, for $\varphi = 0^\circ$, where the external magnetic field is parallel to the c axis, are expected to display an easy-axis behavior by showing the lowest resonance field values. However, as presented by the arrows in Fig. 3, $\mu_0 H_{res}$ shows local maxima instead of a global minimum at $\varphi = 0^\circ, 180^\circ$. As a result, the minimum of $\mu_0 H_{res}$ is shifted by $\pm 35^\circ$ around the local maxima. Hence, the angular response of the uniaxial Co system looks similar to a fourfold cubic anisotropy system, but, as we will discuss in Sec. IV, it arises as a result of the interplay between magnetocrystalline and magnetoelastic anisotropy.

The fourfold anisotropy behavior was observed in the literature for hcp Co, where the hcp grains are oriented in two different orientations, which results in a fourfold anisotropy for Co [26–28]. In Co/GaAs(001), Co grows initially in a cubic body-centered phase, and it transforms into an hcp phase as growth proceeds. However, at lower thickness, a fourfold anisotropy was observed [29]. Also, hcp Co systems are notorious for having fcc stacking faults [14,30,31], which have cubic crystal structure and can show fourfold anisotropy behavior. For the Co films discussed in this article, the PF measurement in Fig. 1(g) shows only one orientation of Co grains. By using reciprocal space mapping, the amount of face-centered-cubic (fcc) phase was estimated to be around 1%, as a result of stacking faults (see Fig. S4 in the Supplemental Material [24]). Such a small amount of fcc phase should not show any significant impact on the angular dependence in FMR of the hcp Co films, as the integrated FMR signal corresponds to the number of magnetic atoms, hence, 1% of cubic Co should not govern the anisotropy curve. So neither the multiple orientations nor the fcc stacking faults of Co can explain the measured angular dependence. Other thicknesses of Co reported in this article also display a similar angular dependence, and are shown in Fig. S4 of the Supplemental Material [24]. First, we will focus on the 75-nm film to better understand the rich FMR angular dependence.

From the FMR measurements, it is clear that the sample does not show bulk-like behavior. Yet to begin with, from Eq. (1), the FMR angular dependence for bulk Co is calculated using the bulk anisotropy constant $K_2 = 0.45\ \mathrm{MJ/m^3}$, as shown by the red curve in Fig. 3. In order to determine the resonance field from the free energy density, together with the magnetoelastic and magnetocrystalline anisotropy energy density discussed in this article, the Zeeman and demagnetization energy density were added to it as well. Solving Baselgia's ferromagnetic resonance condition [25], the ferromagnetic resonance field at various field angles was calculated, as shown in Fig. 3. The model correctly predicts the hard-axis direction. However, the measured anisotropy of the Co films is smaller than the bulk values reported by many authors, e.g., [11,12,14]. The reason for this reduction was claimed to be the presence of stacking faults during the growth [11,14]. In this study, the amount of fcc stacking faults in the volume was determined to be roughly around ∼1%, which is too small for such a strong deviation from bulk anisotropy to be solely explained by stacking faults [14,32].

In order to fit the measured angular dependence, there has to be a source of anisotropy in first place, which counters the magnetocrystalline anisotropy of the hexagonal Co and reduces the overall anisotropy. It is known from the detailed structural characterization that the films are anisotropically strained. Hence, a strain-dependent correction of F_K, i.e. F_{me}, has to be considered. A simplified expression of F_{me} for the Co$(10\bar{1}0)$ orientation was derived in Sec. II. Using the measured strain values from the XRD measurements for the 75-nm-thick Co film in all respective directions, Eq. (3) can be solved as follows:

$$F_{me} = -(-0.139\ \mathrm{MJ/m^3})\cos^2\varphi. \tag{5}$$

The expression is written in the form of Eq. (1), and the magnetoelastic analysis predicts a value with negative sign

for the magnetoelastic anisotropy. This means that the easy axis is perpendicular to the magnetocrystalline anisotropy, and thus reduces it. The effective anisotropy from both mechanisms is described by Eq. (4) and plotted in Fig. 3 as a blue curve, where $K_{2\mathrm{me}} = -0.139\ \mathrm{MJ/m^3}$ and $K_2 = 0.45\ \mathrm{MJ/m^3}$, the bulk Co anisotropy constant, are used to calculate the curve. An inclusion of magnetoelastic anisotropy to the model improves the fitting and predicts the correct behavior at least in the hard-axis direction. However, the discrepancy between experiment and calculated curve is still present in the easy-axis direction, where the model fails in predicting the local maxima along the $\varphi_H = 0^\circ$ direction and instead shows global minima.

As is widely known for the hexagonal Co system, the second-order magnetocrystalline anisotropy constant (K_{22}) is not negligible [33]. Thus, it has to be included in the model. In Sec. II, for a strained sample, F_{me} is the strain-dependent correction of F_K. Hence, it is necessary to consider the second order of F_{me} in our model as well. The magnetocrystalline anisotropy for Co is very well known, where the second-order anisotropy is the next term in the power series expansion [11,15,33]. In contrast, for the second-order magnetoelastic anisotropy term, the change in interatomic distance as a result of strain has to be considered, which already makes the calculation more difficult for the less-symmetric hexagonal system. The calculation of Bruno [17] for F_{me} only considered the strain-dependent correction of first-order magnetocrystalline anisotropy. A proper expression for the second-order term has not been determined to the best of our knowledge. However, for cubic crystals, Kittel [16] has shown comprehensively that in a magnetoelastic equilibrium state, the strain depends on the direction of the magnetization in such a way that the magnetoelastic anisotropy correction can be written in the same symmetry as the magnetocrystalline anisotropy constant. The same result was already shown, for hexagonal systems like Co, in this article in Eq. (4), where the first-order magnetoelastic term has been simplified in the same symmetry as the magnetocrystalline one. Hence, one can express the second-order magnetoelastic anisotropy in the same form as the second-order magnetocrystalline anisotropy. Then, the FMR angular dependence model, as shown in (4), can be rewritten as follows:

$$F_{\mathrm{eff}} = -(K_2 + K_{2\mathrm{me}})\cos^2\varphi - (K_{22} + K_{22\mathrm{me}})\cos^4\varphi, \quad (6)$$

where $K_{22\mathrm{me}}$ is the second-order magnetoelastic anisotropy constant. Furthermore, the above-mentioned fitting model has been used with the known values of $K_{22} = 0.15\ \mathrm{MJ/m^3}$ (bulk anisotropy constant), K_2, and $K_{2\mathrm{me}}$. $K_{22\mathrm{me}}$ was varied until the fitting converged. For $K_{22\mathrm{me}} = -0.22\ \mathrm{MJ/m^3}$, the fitting converges, as shown by the green curve in Fig. 3. The higher negative value of $K_{22\mathrm{me}}$ overcomes K_{22} and thus opposes the easy axis at $\varphi_H = 0^\circ$, which successfully explains a small local maximum along the usual easy direction along the c axis.

So far, the bulk magnetocrystalline anisotropy constant was assumed, but it would be feasible to experimentally determine the value for K_2 from the calculated values of $K_{2\mathrm{me}}$ by Eq. (3). For that, Eq. (6) has to be rewritten as follows, since the symmetry of both anisotropy terms allows it:

$$F_{\mathrm{eff}} = -K_{2\mathrm{eff}}\cos^2\varphi - K_{22\mathrm{eff}}\cos^4\varphi, \quad (7)$$

where

$$K_{2\mathrm{eff}} = K_2 + K_{2\mathrm{me}} \quad (8)$$

is the effective first-order anisotropy constant and

$$K_{22\mathrm{eff}} = K_{22} + K_{22\mathrm{me}} \quad (9)$$

is the effective second-order anisotropy constant. Using Eq. (7), the FMR angular dependence for all the Co thicknesses was fitted (fits are shown in Fig. S4 in the Supplemental Material [24]) and the effective anisotropy constants are plotted in Fig. 4(a). $K_{2\mathrm{eff}}/M$ is positive and decreases as the Co thickness increases, while $K_{22\mathrm{eff}}/M$ remains almost constant at slightly negative anisotropy values for all thicknesses. Now, instead of assuming the bulk-like anisotropy value for K_2/M, its actual values can be calculated. $K_{2\mathrm{eff}}/M$ is known from fitting the FMR results and it is calculated from Eq. (3), using the strain values from Figs. 2(c)–2(e) and the values of B_i's from Table I. Hence, using Eq. (8), the actual K_2/M are extracted and plotted in Fig. 4(b) as black curve for all the Co thicknesses. The K_2/M is very close to the bulk anisotropy constant, as indicated by the dashed horizontal line. This is an important result, as even though the Co films are strained anisotropically, K_2/M remains close to the bulk value over the whole thickness range. Therefore, the magnetoelastic anisotropy energy can be considered as a parasitic modification of the magnetocrystalline anisotropy energy, effectively reducing its overall influence. Similarly, to determine actual values of K_{22}/M, $K_{22\mathrm{me}}/M$ should be known, but, as discussed above, such an expression for $K_{22\mathrm{me}}/M$ is not available. Hence, in this case, K_{22}/M is approximated to its bulk value, since K_2/M is almost equal to the bulk values, and $K_{22\mathrm{me}}/M$ is determined using Eq. (9) and plotted in Fig. 4(c) as a red curve for all Co thicknesses. $K_{22\mathrm{me}}/M$ remains almost constant with relatively large values and thus is responsible for the overall negative sign of $K_{22\mathrm{eff}}/M$.

Variations of the effective anisotropy constants are often related to the axial ratio, c/a, in hcp Co films. Usually for Co films with an OOP c axis orientation, the strain in the basal plane is assumed to be isotropic. It was observed that a compression of the unit cell along the c axis (negative strain) and consequently expansion (positive strain) of the basal plane (via the Poisson effect) results in a magnetoelastic anisotropy [19] which supports the magnetocrystalline anisotropy and finally increases the effective anisotropy constant [34]. Similarly, for an isotropic expansion in the basal plane of IP-oriented Co, the effective anisotropy constant would also increase, and the magnetoelastic anisotropy supports the magnetocrystalline one; see Eq. (A9) in the Appendix. However, for Co films with the c axis in-plane, the basal plane is no longer in the plane of the film but perpendicular to it, and both directions [$a_{[\bar{1}2\bar{1}0]}$ and $d_{[10\bar{1}0]}$, these directions are depicted in Fig. 2(a)] in the basal plane do not have the same strain relaxation mechanism. Hence, the strain in the basal plane should not be assumed isotropic. In this scenario, there are two axial ratios [as shown in Fig. 4(d)], which can influence the effective anisotropy constants in the Co films. Let us refer to them as IP and OOP axial ratios, i.e., $c_{[0001]}/a_{[\bar{1}2\bar{1}0]}$ and $c_{[0001]}/d_{[10\bar{1}0]}$, respectively. To determine the correlation of $F_{\mathrm{me}}^{10\bar{1}0}$ with the axial ratios, Eq. (3) can be simplified as follows

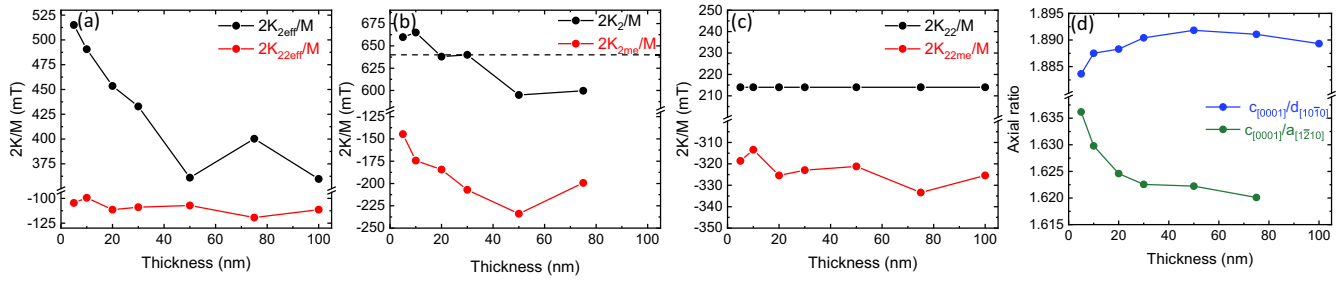

FIG. 4. (a) First-order ($2K_{2\text{eff}}/M$) and second-order ($2K_{22\text{eff}}/M$) effective anisotropy field as determined from FMR as a function of thickness. (b) First-order and (c) second-order magnetocrystalline anisotropy field ($2K_2/M$, $2K_{22}/M$) and magnetoelastic anisotropy field ($2K_{2\text{me}}/M$, $2K_{22\text{me}}/M$) as a function of thickness, where M is the saturation magnetization of Co. (b) The dashed line indicates the Co bulk value for $2K_2/M$. (d) Two, OOP and IP, axial ratios are shown; the dimensions are as highlighted in Fig. 2(a). The ones in green and blue are referred to as IP and OOP axial ratios, respectively.

(see the Appendix for details):

$$F_{\text{me}}^{(10\bar{1}0)} = \frac{\sin^2\varphi}{8c_{13}}((11B_1c_{13} - 8B_2c_{13} + 8B_3c_{13})\ _{yy} + (-3B_1c_{13} + 8B_3c_{13} - 8B_2c_{33})\ _{zz}), \quad (10)$$

where c_{ij} are the elastic stiffness constants. The positive tensile strain ($_{yy} > 0$) along $[\bar{1}2\bar{1}0]$ increases $a_{[\bar{1}2\bar{1}0]}$, thereby decreasing the IP axial ratio. The influence of this change on $F_{\text{me}}^{(10\bar{1}0)}$ is measured as $\partial F_{\text{me}}^{(10\bar{1}0)}/\partial\ _{yy} = 46.0625\ \text{MJ/m}^3$. The positive slope contributes to an increase of $F_{\text{me}}^{(10\bar{1}0)}$, which in turn enhances F_K. The OOP axial ratio increases as a result of OOP compressive strain ($_{zz} < 0$) along $[10\bar{1}0]$ reducing $d_{[10\bar{1}0]}$. The strength of influence of the OOP axial ratio on $F_{\text{me}}^{(10\bar{1}0)}$ is measured as $\partial F_{\text{me}}^{(10\bar{1}0)}/\partial\ _{zz} = -132.034\ \text{MJ/m}^3$. The roughly three times higher negative slope decreases $F_{\text{me}}^{(10\bar{1}0)}$ about three times more strongly than the prior one. This leads to an overall reduction of F_K. As a result, the uniaxial anisotropy constants deviate strongly from their bulk values. Therefore, it is the OOP axial ratio or OOP strain, that strongly controls $F_{\text{me}}^{(10\bar{1}0)}$ and is responsible for the negative sign of the magnetoelastic anisotropy constants. By exploiting control over the strain through improved crystallographic engineering of given IP Co films, even higher IP uniaxial anisotropy could be achieved, paving the way for exciting developments in spintronic research and applications.

V. SUMMARY

We presented a thickness variation of Co films with their crystallographic c axis lying in the film plane. This gives rise to an IP uniaxial anisotropy. The detailed structural characterization reveals that the films' lattice remains strained even for thicker films. A very large lattice mismatch in one of the lateral directions of the Cr(112) layer is one possible reason for the observed strain. Furthermore, FMR measurements reveal an unexpected fourfold-like anisotropy for this commonly uniaxial system of hcp Co. The magnetoelastic analysis successfully explains the results of the FMR measurements. It predicts that, for a given strain, the magnetoelastic anisotropy energy counteracts the magnetocrystalline anisotropy, as its easy axis is oriented perpendicular to the magnetocrystalline one. Additional decomposition of $F_{\text{me}}^{10\bar{1}0}$ reveals that the OOP compressive strain has the strongest influence on it. Hence, it effectively reduces the measured anisotropy constants. So far, such reduction in anisotropy was assumed to be solely a result of fcc-stacking faults, but here it is clearly shown that the magnetoelasticity strongly influences the magnetic anisotropy energy even at Co layer thicknesses of up to 100 nm.

ACKNOWLEDGMENTS

The authors gratefully acknowledge Rico Ehrler for his assistance with multiple IP-XRD measurements conducted at TU Chemnitz and Andreas Worbs for TEM specimen preparation at HZDR. Work at nanoGUNE was supported by the Spanish Ministry of Science and Innovation under the Maria de Maeztu Units of Excellence Programme (Grant No. CEX2020-001038-M), Project No. PID2021-123943NB-I00 (OPTOMETAMAG), and the predoctoral fellowship No. PRE2019-088428. Support by the Structural Characterization Facilities Rossendorf at IBC is gratefully acknowledged.

APPENDIX: AN EXPRESSION FOR THE MAGNETOELASTIC ANISOTROPY ENERGY DENSITY FOR Co($10\bar{1}0$)

The calculation of the magnetoelastic anisotropy in Co is illustrated below. Only the first-order term of the magnetocrystalline anisotropy was used by Bruno in determining the expression of the magnetoelastic anisotropy for (0001)-oriented Co [17]:

$$F_{\text{me}}^{(0001)} = B_1\left(\alpha_x^2\ _{xx} + 2\alpha_x\alpha_y\ _{xy} + \alpha_y^2\ _{yy}\right) + B_2\left(1-\alpha_z^2\right)\ _{zz} + B_3\left(1-\alpha_z^2\right)(\ _{xx} +\ _{yy}) + B_4(2\alpha_y\alpha_z\ _{yz} + 2\alpha_x\alpha_z\ _{xz}), \quad (A1)$$

TABLE I. The magnetoelastic coupling constants B_i are given in MJ/m^3, while the elastic stiffness constants c_{ij} are given in GPa for hcp Co [35].

Parameter	B_1	B_2	B_3	B_4	c_{11}	c_{12}	c_{44}	c_{13}	c_{33}
Value	−8.1	−29	28.2	37.4	307	165	75.5	103	358

where, α_i's are the directions cosines of the applied magnetic field. For hexagonal symmetry, the elastic energy is written as follows:

$$F_{\text{el}} = \tfrac{1}{2}c_{11}\left(\varepsilon_{xx}^2 + \varepsilon_{yy}^2\right) + \tfrac{1}{2}c_{33}\,\varepsilon_{zz}^2 + c_{12}\,\varepsilon_{xx}\,\varepsilon_{yy} + c_{13}(\varepsilon_{xx}\,\varepsilon_{zz} + \varepsilon_{yy}\,\varepsilon_{zz}) + 2c_{44}\left(\varepsilon_{yz}^2 + \varepsilon_{xz}^2\right) + (c_{11} - c_{12})\,\varepsilon_{xy}^2, \tag{A2}$$

where c_{ij} are the elastic stiffness constants.

Following the method by Sander [18], one can derive the magnetoelastic anisotropy energy in $(10\bar{1}0)$-oriented Co. For that, the coordinate transformation matrix between the (0001)- and $(10\bar{1}0)$-oriented planes is

$$a_{ij} = \begin{pmatrix} 0 & 0 & 1 \\ \frac{-1}{\sqrt{2}} & \frac{\sqrt{3}}{2} & 0 \\ \frac{-\sqrt{3}}{2} & \frac{-1}{\sqrt{2}} & 0 \end{pmatrix}. \tag{A3}$$

Hence, Eq. (A2) could be rewritten for $\text{Co}(10\bar{1}0)$ by transforming the strain tensor to the primed coordinate system:

$$\varepsilon'_{ij} = a_{ik}\,\varepsilon_{kl}\,a_{lj}. \tag{A4}$$

Here, the primed strain tensor is in the coordinate system of $(10\bar{1}0)$-oriented planes. Minimizing the elastic energy with respect to ε'_{xx} by solving $\partial F_{\text{el}}/\partial\,\varepsilon'_{xx} = 0$ yields

$$\varepsilon'_{xx} = \frac{-c_{12}\,\varepsilon_{yy} - c_{11}\,\varepsilon_{zz}}{c_{13}}. \tag{A5}$$

Similarly, to write the magnetocrystalline anisotropy energy for $\text{Co}(10\bar{1}0)$, the direction cosines from Eq. (A1) are required to be rewritten in the coordinate system of the $(10\bar{1}0)$ plane, as follows:

$$\alpha_i = a_{ij}\alpha_j. \tag{A6}$$

Substituting it in (A1) yields the magnetoelastic anisotropy energy for $\text{Co}(10\bar{1}0)$,

$$F_{\text{me}}^{(10\bar{1}0)} = B_2\left(1 - \alpha_x^2\right)\varepsilon'_{xx} + B_3\left(1 - \alpha_x^2\right)(\varepsilon_{yy} + \varepsilon_{zz}) \times \tfrac{1}{8}B_1\left(\alpha_y^2(11\,\varepsilon_{yy} - 3\,\varepsilon_{zz}) + 2\sqrt{3}\alpha_y\alpha_z(\varepsilon_{yy} - \varepsilon_{zz}) + \alpha_z^2(-3\,\varepsilon_{yy} + 11\,\varepsilon_{zz})\right). \tag{A7}$$

In this article, the experiment focuses on the in-plane measurements, hence substituting $\alpha_z = 0$ in (A7) and also using $\alpha_x = \cos\varphi$ and $\alpha_y = \sin\varphi$ for $\theta = \pi/2$. Equation (A7) could be simplified as follows:

$$F_{\text{me}}^{(10\bar{1}0)} = \tfrac{1}{8}(8B_2\,\varepsilon'_{xx} + B_1(11\,\varepsilon_{yy} - 3\,\varepsilon_{zz}) + 8B_3(\varepsilon_{yy} + \varepsilon_{zz}))\sin^2\varphi. \tag{A8}$$

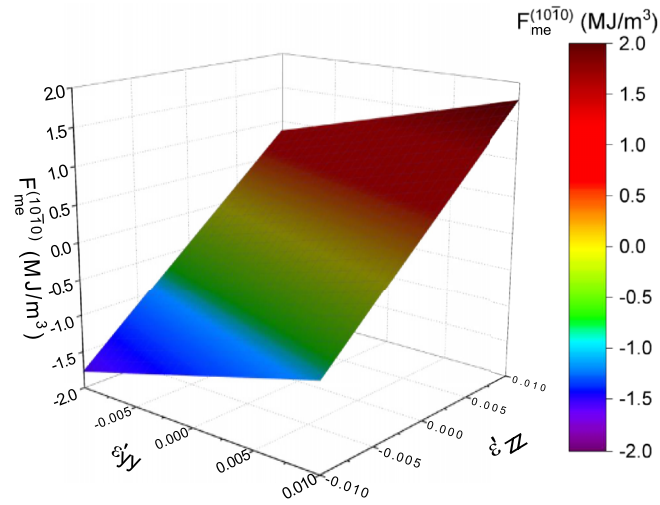

FIG. 5. Calculated $F_{\text{me}}^{10\bar{1}0}$ for strain in the basal plane.

Further, we derive a special case where strain in the basal plane, i.e., (0001), is isotropic, meaning $\varepsilon_{yy} = \varepsilon_{zz} = \varepsilon_0$:

$$F_{\text{me}}^{(10\bar{1}0)} = (B_2\,\varepsilon_{xx} + (B_1 + 2B_3)\,\varepsilon_0)\sin^2\varphi = (-29\,\varepsilon_{xx} + 48.3\,\varepsilon_0)\sin^2\varphi \tag{A9}$$

The values for B_i are taken from Table I, and F_{me} is given in MJ/m^3. We note that Eq. (A9) is exactly of the same form as the one for the isotropic case in the basal plane for OOP-oriented Co films [19]. For this case—compression of the unit cell in c axis direction and uniform expansion of the basal plane, or in other words, reduction of the c/a ratio—the easy axis of F_{me} supports F_K and an increase of K_{eff} is reported [34].

In case of anisotropic strain in the basal plane of Co films ($\varepsilon_{yy} \neq \varepsilon_{zz}$), which is the scenario of this article, the lattice parameters of the basal planes are now different; hence, instead of one, there are two axial ratios that can influence the effective anisotropy constants. To understand that, one can further simplify Eq. (A8) using Eq. (A5):

$$F_{\text{me}}^{(10\bar{1}0)} = \frac{\sin^2\varphi}{8c_{13}}((11B_1c_{13} - 8B_2c_{13} + 8B_3c_{13})\,\varepsilon_{yy} + (-3B_1c_{13} + 8B_3c_{13} - 8B_2c_{33})\,\varepsilon_{zz}). \tag{A10}$$

Using the known values of B_i and c_{ij} for bulk Co, Eq. (A10) is plotted in Fig. 5. The slope for the OOP strain in the basal plane, $\partial F_{\text{me}}^{10\bar{1}0}/\partial\,\varepsilon_{zz} = -132.034\ \text{MJ/m}^3$, is almost three times smaller than the strain in the basal plane, $\partial F_{\text{me}}^{10\bar{1}0}/\partial\,\varepsilon_{yy} = 46.0625\ \text{MJ/m}^3$. This clearly indicates that any small variation of ε_{zz} strongly influences the anisotropy. Also, Fig. 5 shows the strong variation of $F_{\text{me}}^{(10\bar{1}0)}$ with respect to ε_{zz} compared to ε_{yy}.

[1] W. Sucksmith and J. E. Thompson, The magnetic anisotropy of cobalt, Proc. R. Soc. London A **225**, 362 (1954).

[2] H. P. J. Wijn, *Magnetic Properties of Metals: d-Elements, Alloys and Compounds* (Springer, Berlin, 1991), pp. 1–21.

[3] M. N. Baibich, J. M. Broto, A. Fert, F. Nguyen Van Dau, F. Petroff, P. Etienne, G. Creuzet, A. Friederich, and J. Chazelas, Giant magnetoresistance of (001)Fe/(001)Cr magnetic superlattices, Phys. Rev. Lett. **61**, 2472 (1988).

[4] B. Dieny, I. L. Prejbeanu, K. Garello, P. Gambardella, P. Freitas, R. Lehndorff, W. Raberg, U. Ebels, S. O. Demokritov, J. Akerman, A. Deac, P. Pirro, C. Adelmann, A. Anane, A. V. Chumak, A. Hirohata, S. Mangin, S. O. Valenzuela, M. C. Onbaşlı, M. d'Aquino *et al.*, Opportunities and challenges for spintronics in the microelectronics industry, Nat. Electron. **3**, 446 (2020).

[5] Z. Guo, J. Yin, Y. Bai, D. Zhu, K. Shi, G. Wang, K. Cao, and W. Zhao, Spintronics for energy- efficient computing: An overview and outlook, Proc. IEEE **109**, 1398 (2021).

[6] I. M. Miron, K. Garello, G. Gaudin, P.-J. Zermatten, M. V. Costache, S. Auffret, S. Bandiera, B. Rodmacq, A. Schuhl, and P. Gambardella, Perpendicular switching of a single ferromagnetic layer induced by in-plane current injection, Nature (London) **476**, 189 (2011).

[7] V. Krizakova, M. Perumkunnil, S. Couet, P. Gambardella, and K. Garello, Spin-orbit torque switching of magnetic tunnel junctions for memory applications, J. Magn. Magn. Mater. **562**, 169692 (2022).

[8] Q. Shao, P. Li, L. Liu, H. Yang, S. Fukami, A. Razavi, H. Wu, K. Wang, F. Freimuth, Y. Mokrousov, M. D. Stiles, S. Emori, A. Hoffmann, J. Akerman, K. Roy, J.-P. Wang, S.-H. Yang, K. Garello, and W. Zhang, Roadmap of spin–orbit torques, IEEE Trans. Magn. **57**, 1 (2021).

[9] S. Nallan and J.-G. Zhu, Achieving uniaxial in-plane magnetocrystalline anisotropy to enable scalable SOT-MRAM devices, in *2023 IEEE International Magnetic Conference - Short Papers* (IEEE, Piscataway, NJ, 2023).

[10] S. Nallan and J.-G. Zhu, Spin Hall switching enabled by uniaxial in-plane magnetocrystalline anisotropy, IEEE Trans. Magn. **59**, 1 (2023).

[11] W. Yang, D. N. Lambeth, and D. E. Laughlin, Unicrystal Co–alloy media on Si(110), J. Appl. Phys. **85**, 4723 (1999).

[12] W. Yang, D. N. Lambeth, and D. E. Laughlin, Dependence of Co anisotropy constants on temperature, processing, and underlayer, J. Appl. Phys. **87**, 6884 (2000).

[13] A. Nakamura, M. Koguchi, and M. F. Masaaki Futamoto, Microstructures of Co/Cr bilayer films epitaxially grown on MgO single-crystal substrates, Jpn. J. Appl. Phys. **34**, 2307 (1995).

[14] Y. Liu, M. D. Kitcher, M. De Graef, and V. Sokalski, Towards hexagonal C_2 systems with anisotropic Dzyaloshinkii-Moriya interaction: Characterization of epitaxial Co$(10\bar{1}0)$/Pt(110) multilayer films, Phys. Rev. Mater. **5**, L101401 (2021).

[15] J. A. Arregi, J. B. Gonzalez-Diaz, O. Idigoras, and A. Berger, Strain-induced magneto-optical anisotropy in epitaxial hcp Co films, Phys. Rev. B **92**, 184405 (2015).

[16] C. Kittel, Physical theory of ferromagnetic domains, Rev. Mod. Phys. **21**, 541 (1949).

[17] P. Bruno, Magnetic surface anisotropy of Cobalt and surface roughness effects within Neel's model, J. Phys. F **18**, 1291 (1988).

[18] D. Sander, The correlation between mechanical stress and magnetic anisotropy in ultrathin films, Rep. Prog. Phys. **62**, 809 (1999).

[19] D. Sander, The magnetic anisotropy and spin reorientation of nanostructures and nanoscale films, J. Phys.: Condens. Matter **16**, R603 (2004).

[20] O. Idigoras, A. K. Suszka, P. Vavassori, B. Obry, B. Hillebrands, P. Landeros, and A. Berger, Magnetization reversal of in-plane uniaxial Co films and its dependence on epitaxial alignment, J. Appl. Phys. **115**, 083912 (2014).

[21] K. Heinz, S. Müller, and L. Hammer, Crystallography of ultrathin iron, cobalt and nickel films grown epitaxially on copper, J. Phys.: Condens. Matter **11**, 9437 (1999).

[22] T. Kawabe, Perceptual properties of the Poisson effect, Front. Psychol. **11**, 612368 (2021).

[23] S. Kobayashi, X-ray thin-film measurement techniques: In-plane XRD measurement, Rigaku J., **26**, 3 (2010).

[24] See Supplemental Material at http://link.aps.org/supplemental/10.1103/PhysRevB.111.054431 for IP-XRD scans in both IP directions, cross-sectional bright-field TEM images and RSM of 75-nm-thick Co film, and IP angular FMR measurement with the fitting based on the model discussed in Eq. (7).

[25] L. Baselgia, M. Warden, F. Waldner, S. L. Hutton, J. E. Drumheller, Y. Q. He, P. E. Wigen, and M. Marysko, Derivation of the resonance frequency from the free energy of ferromagnets, Phys. Rev. B **38**, 2237 (1988).

[26] M. Z. Xue, S. L. Ding, R. Wu, L. Zha, G. Y. Qiao, H. L. Du, J. Z. Han, Y. C. Yang, C. S. Wang, and J. B. Yang, Thickness induced uniaxial anisotropy and unexpected four-fold symmetry in Co/SiO_2/Si films, AIP Adv. **8**, 056311 (2017).

[27] J. F. Calleja, M. García del Muro, B. Presa, R. Matarranz, J. A. Corrales, A. Labarta, and M. C. Contreras, Fourfold magnetic anisotropy, coercivity and magnetization reversal of Co/V bilayers grown on MgO(001), J. Phys. D **40**, 6857 (2007).

[28] E. Gu, M. Gester, R. J. Hicken, C. Daboo, M. Tselepi, S. J. Gray, J. A. C. Bland, L. M. Brown, T. Thomson, and P. C. Riedi, Fourfold anisotropy and structural behavior of epitaxial hcp Co/GaAs(001) thin films, Phys. Rev. B **52**, 14704 (1995).

[29] M. Madami, S. Tacchi, G. Gubbiotti, G. Carlotti, and G. Socino, Thickness dependence of magnetic anisotropy in ultrathin Co/GaAs(001) films, Surf. Sci. **566-568**, 246 (2004).

[30] G. Patel, F. Ganss, R. Salikhov, S. Stienen, L. Fallarino, R. Ehrler, R. A. Gallardo, O. Hellwig, K. Lenz, and J. Lindner, Structural and magnetic properties of thin Cobalt films with mixed hcp and fcc phases, Phys. Rev. B **108**, 184429 (2023).

[31] V. Sokalski, D. E. Laughlin, and J.-G. Zhu, Magnetic anisotropy and stacking faults in Co and $Co_{84}Pt_{16}$ epitaxially grown thin films, J. Appl. Phys. **110**, 093919 (2011).

[32] C. J. Aas, L. Szunyogh, R. F. L. Evans, and R. W. Chantrell, Effect of stacking faults on the magnetocrystalline anisotropy of hcp Co: A first-principles study, J. Phys.: Condens. Matter **25**, 296006 (2013).

[33] R. M. Bozorth, Magnetostriction and crystal anisotropy of single crystals of hexagonal Cobalt, Phys. Rev. **96**, 311 (1954).

[34] J.-J. Wang, T. Sakurai, K. Oikawa, K. Ishida, N. Kikuchi, S. Okamoto, H. Sato, T. Shimatsu, and O. Kitakami, Magnetic anisotropy of epitaxially grown Co and its alloy thin films, J. Phys.: Condens. Matter **21**, 185008 (2009).

[35] D. Sander, Magnetostriction and magnetoelasticity, in *Handbook of Magnetism and Magnetic Materials* (Springer International, Cham, 2020), pp. 1–45.